IOPscience iopscience.iop.org

Home Search Collections Journals About Contact us My IOPscience

Optical spectra and crystal field calculations of Nd^{3+} doped Zircon-type YMO_4 laser hosts ($M = V$, P, As)

This article has been downloaded from IOPscience. Please scroll down to see the full text article.

1998 J. Phys.: Condens. Matter 10 6491

(http://iopscience.iop.org/0953-8984/10/29/009)

View the table of contents for this issue, or go to the journal homepage for more

Download details:
IP Address: 171.66.16.209
The article was downloaded on 14/05/2010 at 16:37

Please note that terms and conditions apply.

J. Phys.: Condens. Matter **10** (1998) 6491–6503. Printed in the UK PII: S0953-8984(98)92229-9

Optical spectra and crystal field calculations of Nd^{3+} doped Zircon-type YMO_4 laser hosts (M = V, P, As)

O Guillot-Noël†, A Kahn-Harari†, B Viana†, D Vivien†, E Antic-Fidancev‡ and P Porcher‡

† Chimie Appliquée de l'Etat Solide, ENSCP, CNRS-UMR 7574, 11 rue Pierre et Marie Curie, F-75231 Paris Cédex 05, France

‡ Chimie Métallurgique des Terres Rares, UPR 209, 1 Place Aristide Briand, 92195 Meudon Cédex, France

Received 4 March 1998

Abstract. Low temperature absorption spectra of Nd^{3+} doped YVO_4, YPO_4 and $YAsO_4$ single crystals, grown by the flux method, are reported. A simulation of the energy level scheme is carried out. The effective Hamiltonian includes elementary interactions such as coulombic, spin–orbit, two- and three-body interactions. The crystal field effect is introduced through the five non-zero crystal field parameters allowed by the D_{2d} symmetry site occupied by the rare earth. A simulation is performed on the 96 (102, 90) experimental energy levels of YVO_4, (YPO_4, $YAsO_4$) with a good rms standard deviation of 16.2 (15.4, 15.7) cm^{-1}. It is noteworthy that the energy level scheme of $YAsO_4$ is reported for the first time. The wave functions of the systems are used for the calculation of the magnetic factor g. These factors are in good agreement with the values deduced from EPR measurements on the Nd^{3+} lowest level $^4I_{9/2}$. The crystal field parameters are also compared to the *a priori* parameters calculated using the simple overlap model and the correlated crystal field strength is also analysed.

1. Introduction

Nd:YVO_4 with zircon-type structure has found renewed interest in the last years as a laser material [1–4]. This is mainly due to strong absorption and emission cross sections. Nd:$GdVO_4$ presents similar optical features though with a few differences on the cross section intensity and crystal field strength [5] (for the $^4F_{3/2}$ emitting level, the energy levels splittings are $\Delta E = 6$ cm^{-1} for Nd:$GdVO_4$ and 18 cm^{-1} for Nd:YVO_4). The Nd^{3+} 810 nm broad absorption band observed at room temperature can be explained by the relatively small crystal field strength in these matrices [6]. In isostructural compounds i.e. YPO_4, $YAsO_4$, Nd^{3+} ions present properties close to those found in YVO_4 [6]. Moreover, to our knowledge, the spectroscopic characteristics of Nd^{3+}:$YAsO_4$ have not yet been reported in the literature. Then, it appeared of interest to compare the energy level schemes derived from experiment and their simulation within the crystal field (cf) theory frame. Moreover, the knowledge of a numerical expression of the wave functions associated with each level offers the opportunity to calculate physicochemical properties in which they are involved such as g tensor principal values, deduced from EPR measurements. A comparison in the series provides an interesting test of the validity of the model.

0953-8984/98/296491+13$19.50 © 1998 IOP Publishing Ltd

2. Crystallographic background

YVO_4, YPO_4 and $YAsO_4$ belong to the zircon-type structure ($ZrSiO_4$, also called xenotime), with tetragonal symmetry. The space group is $I4_1/amd$, with four formula units in the unit cell. In this host lattice, Y^{3+} ions are eightfold coordinated by oxygen ions, forming $[YO_8]$ dodecahedra, and the $[MO_4]$ group is a distorted tetrahedron. The structure can be described as chains parallel to the c axis of alternating edge-sharing $[MO_4]$ tetrahedra and $[YO_8]$ dodecahedra (figure 1). $[YO_8]$ can also be viewed as two interlaced tetrahedra. The optically active neodymium ion is located on the Y^{3+} position with a D_{2d} site symmetry (figure 1). With respect to the effective ionic radii of the various M ions involved in the $[MO_4]$ group (table 1), one can expect rather similar arrangements of bond lengths and angles for the three hosts.

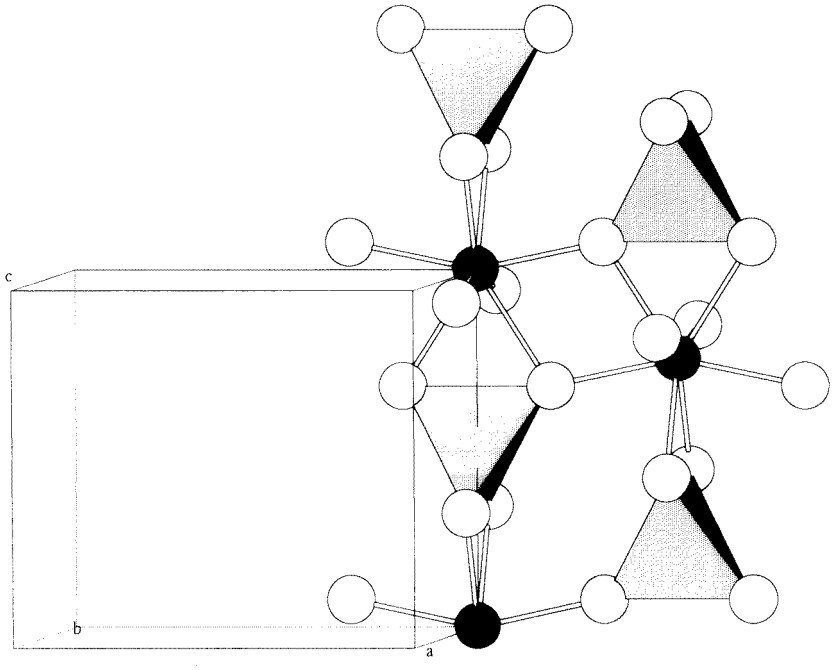

Figure 1. Tetragonal unit cell of YMO_4 (M = V, P, As). MO_4 groups are schematically represented by tetrahedra; oxygen ions around the central yttrium of YO_8 polyhedra are also indicated. Nd^{3+} doping ions lie on the Y^{3+} sites. (Empty circles are O^{2-} and black circles are Y^{3+}.)

3. Experiment

3.1. Single crystal elaboration

The crystal growth was performed by the flux method, which is the most appropriate for compounds having either non-congruent melting or very high melting points. Moreover, one supplementary limitation was to elaborate crystals of the three matrices in conditions as similar as possible, in order to make the most realistic comparisons in the crystal series.

Table 1. Structural parameters of YMO_4 (M = V, P, As) zircon matrices.

YMO_4 $I4_1/amd$	Tetragonal unit cell parameters (Å)	M ionic radius (Å)	O–Y distances (Å)	O–Y–O angles (°)
YVO_4	$a = 7.119$	0.355	2.30 (×4)	156.0
	$c = 6.289$		2.43 (×4)	63.3
$YAsO_4$	$a = 7.044$	0.335	2.300 (×4)	155.6
	$b = 6.248$		2.412 (×4)	63.8
YPO_4	$a = 6.888$	0.17	2.313 (×4)	152.7
	$b = 6.021$		2.374 (×4)	60.5

The crystal growth of all three YMO_4 hosts (M = V, P, As) was performed with a $Pb_2M_2O_7$ flux [7, 8], according to the general chemical reaction:

$$y\mathrm{Pb_2M_2O_7} + x\mathrm{Y_2O_3} \rightarrow 2x\mathrm{YMO_4} + 2x\mathrm{PbO} + (y - x)\mathrm{Pb_2M_2O_7}.$$

This is not a simple flux/compound system, since the final product is prepared at the expense of the flux itself. Therefore, it forms a rather complex system in which the relative proportions of PbO/M_2O_5 vary during the crystal growth. In order to improve the viscosity and the dissolving power of the flux, two more salts, MoO_3 and PbF_2, were added to the basic $Pb_2M_2O_7$ flux. All three compounds were prepared with 1% of doping Nd^{3+} ions.

The heating process was as follows: first, the starting powders $Pb_2M_2O_7$, MoO_3, PbF_2 and Y_2O_3 were mixed and compressed as pellets, then introduced into a platinum crucible. The nominal compositions were approximately 60 wt% $Pb_2M_2O_7$, 6 wt% $Y_2O_3 + Nd_2O_3$, 30 wt% MoO_3 and 2 wt% PbF_2. Then the temperature was raised to 1270 °C, at which fusion was achieved. After a soaking period of 12 h to ensure the dissolution and homogenization of Y_2O_3 in the melt, a slow cooling (2 °C h^{-1}) from 1270 °C to 800 °C produced the precipitation of expected Nd:YMO_4 crystals from the melt.

The crystals are easily separated by selective dissolution of the flux in dilute nitric acid. When performed in a relatively large crucible (100 cm^3) they are well shaped, as rods or platelets with several mm^2 area and 1–2 mm thickness. In the crystals, large, clear and transparent zones are selected in which oriented slices are cut and polished to perform the optical studies reported hereafter. A browning of Nd:YVO_4 crystals was observed in contact with air or light, which has no influence on the optical behaviour of the Nd^{3+} ions.

3.2. Optical measurements

The absorption spectra were recorded at 4.2 K on a Cary 5-Varian spectrometer equipped with an Oxford Instruments helium flow cryostat, operating in the 180–3200 nm wavelength range. The near infrared fluorescence measurements were performed using a SOPRA SP-750 monochromator and a PbS cell associated with a lock-in amplifier. The excitation wavelength is selected at 810 nm from a cw titanium sapphire laser pumped by a 7 W argon ion laser.

3.3. EPR measurements

The EPR measurements were performed at X-band using a Bruker ER 220D spectrometer equipped with a liquid helium cryostat from Oxford Instruments. The crystals were mounted on a small Perspex sample holder in order to allow their orientation with respect to the magnetic field. The frequency was measured by a Systron Donner frequency-counter.

4. Results and discussion

4.1. Simulation of the energy level position

From the optical absorption spectra recorded at low temperature, all electronic transitions assigned to Nd^{3+} ions in the three hosts originate from the lowest Stark component of the $^4I_{9/2}$ level. In the case of Nd^{3+} ions in YVO_4 and $YAsO_4$, some extra lines in the spectra (figure 2) are assigned to vibronic side bands, associated with electronic transitions. All of them are located in the hypersensitive transition area, at 580 nm [9, 10]. A few other extra lines are also observed. Their positions are in agreement with those indicated in [11]. They correspond to Nd^{3+} ions perturbed by the presence of other Nd^{3+} ions in their vicinity. These Nd–Nd pairs can be evidenced by EPR measurement even at very low Nd^{3+} concentration (less than 1%).

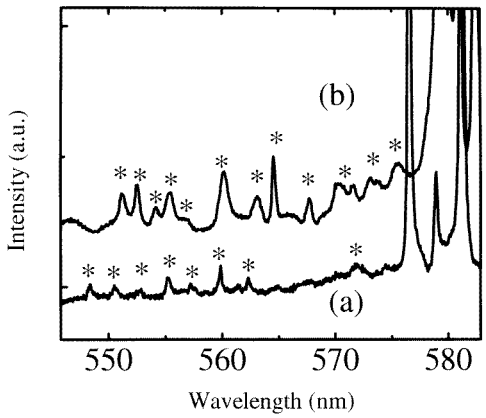

Figure 2. Absorption spectra for Nd^{3+} ions in the vicinity of the $^4I_{9/2} \rightarrow {}^4G_{7/2}+{}^2K_{13/2}+{}^4G_{9/2}$ transition at 10 K in (a) $YAsO_4$, (b) YVO_4. The lines labelled by a star are vibronic transitions, which are not taken into account in the crystal field calculation.

For Nd^{3+} ions, almost only the $^4F_{3/2}$ level emits. The cf splittings of this level are $\Delta E = 18\ cm^{-1}$, $26\ cm^{-1}$ and $51\ cm^{-1}$ respectively for YVO_4, $YAsO_4$ and YPO_4. The $^4F_{3/2}$ level splitting being known from absorption, it is easy to determine the five (six) crystal field components of $^4I_{9/2}$ ($^4I_{11/2}$) from the $^4F_{3/2} \rightarrow {}^4I_{9/2}$ and $^4F_{3/2} \rightarrow {}^4I_{11/2}$ transitions (figures 3(a) and (b)). The experimental energy levels obtained from the low temperature absorption and emission measurements are listed in table 2.

Although all interactions are included together in the secular determinant, it is more convenient for the description to separate the interactions operating between the elementary states of a configuration into two parts: first, the free-ion interactions are written according to the formalism of Carnall *et al* [12]:

$$H_{FI} = H_0 + \sum_{k=0,1,2,3} E^k(nf, nf)e_k + \zeta_{4f}A_{SO} + \alpha L(L+1) + \beta G(G_2) + \gamma G(R_7) + \sum_{\lambda=2,3,4,6,7,8} T^\lambda t_\lambda. \quad (1)$$

In this expression, E^k are the Racah parameters, ζ_{4f} is the spin–orbit coupling constant. e_k and A_{SO} represent the angular parts of the electrostatic repulsion and spin–orbit coupling respectively. α, β and γ are associated with the two-body interactions and the T^λ (Judd

Table 2. Energy levels (cm^{-1}) of Nd^{3+} in YVO_4, $YAsO_4$, and YPO_4 single crystals (* levels not considered in this adjustment).

$^{2S+1}L_J$	YVO_4		$YAsO_4$		YPO_4	
levels	E (exp.)	E (cal.)	E (exp.)	E (cal.)	E (exp.)	E (cal.)
$^4I_{9/2}$	0	3	0	6	0	0
	110	130	111	133	117	129
	173	197	192	194	215	247
	228	243	232	249	293	250
	437	453	366	388	403	413
$^4I_{11/2}$	1 966	1 958	1 977	1 963	1 989	1 981
	1 987	1 980	2 003	1 987	2 023	2 019
	2 046	2 047	2 042	2 037	2 050	2 043
	2 067	2 064	2 068	2 066	2 059	2 057
	2 157	2 158	2 123	2 123	2 141	2 140
	2 180	2 177	2 147	2 145	2 177	2 173
$^4I_{13/2}$	3 908	3 895	3 933	3 916	3 931	3 926
	3 931	3 918	3 944	3 928	3 973	3 958
	3 977	3 975	3 989	3 981	4 004	3 997
	4 042	4 042	—	4 049	4 030	4 034
	4 087	4 086	4 056	4 056	4 066	4 062
	4 157	4 151	4 125	4 128	4 151	4 152
	4 159	4 163	4 131	4 128	4 160	4 157
$^4I_{15/2}$	5 831	5 822	5 875	5 876	5 829	5 834
	5 868	5 869	5 885	5 883	5 925	5 918
	5 917	5 918	5 947	5 945	—	5 965
	6 064	6 070	6 059	6 065	6 080	6 086
	—	6 183	—	6 185	—	6 172
	—	6 250	6 217	6 220	6 247	6 248
	6 261	6 265	—	6 222	—	6 255
	6 317	6 316	6 279	6 277	6 316	6 317
$^4F_{3/2}$	11 368	11 344	11 414	11 402	11 413	11 410
	11 386	11 370	11 440	11 428	11 464	11 445
$^4F_{5/2}$	12 362	12 331	12 424	12 399	12 428	12 430
	12 400	12 383	12 454	12 436	12 447	12 430
+	12 411	12 415	12 468	12 479	12 466	12 493
	12 479	12 501	12 501	12 545	12 475	12 545
$^2H2_{9/2}$	12 496	12 540	12 548	12 569	12 494	12 555
	12 536	12 542	12 595	12 575	12 523	12 615
	12 600	12 652	12 638	12 668	12 587	12 671
	12 686	12 661	12 710	12 684	12 728	12 718
$^4F_{7/2}$	13 318	13 325	13 378	13 390	13 373	13 387
+	13 341	13 344	13 398	13 405	13 388	13 404
$^4S_{3/2}$	13 392	13 397	13 422	13 439	13 483	12 491
	13 457	13 441	13 503	13 504	—	13 505
	13 464	13 449	13 506	13 510	13 519	13 525
	—	13 471	13 511	13 512	—	13 525
$^4F_{9/2}$	14 572	14 567	14 635	14 633	14 639	14 640
	14 593	14 587	14 646	14 645	—	14 643
	14 629	14 626	14 680	14 685	14 730	14 728
	14 713	14 705	14 759	14 756	14 762	14 763
	14 736	14 733	14 772	14 777	—	14 768

Table 2. (Continued)

$^{2S+1}L_J$ levels	YVO_4		$YAsO_4$		YPO_4	
	E (exp.)	*E* (cal.)	*E* (exp.)	*E* (cal.)	*E* (exp.)	*E* (cal.)
$^2H2_{11/2}$ *	15 764	15 773	15 814	15 828	15 817	15 834
	15 798	15 787	15 846	15 839	15 850	15 844
	15 854	15 803	—	15 856	15 895	15 863
	—	15 814	15 896	15 861	15 903	15 874
	15 932	15 814	15 972	15 862	—	15 882
	15 966	15 841	16 000	15 883	16 008	15 891
$^2G1_{7/2}$	16 824	16 823	16 968	16 971	16 985	16 982
	16 958	16 975	17 054	17 065	17 065	17 052
+	16 976	17 000	17 117	17 111	17 115	17 116
	17 170	17 172	17 205	17 210	17 210	17 218
$^4G_{5/2}$	17 205	17 193	—	17 228	—	17 232
	—	17 234	17 273	17 284	17 285	17 297
	17 251	17 239	17 344	17 313	17 356	17 321
$^4G_{7/2}$	18 744	18 747	18 897	18 855	—	18 844
	18 834	18 817	18 937	18 908	18 891	18 915
+	18 856	18 865	18 970	18 961	18 963	18 953
	18 922	18 935	19 009	19 007	19 030	19 023
$^2K_{13/2}$	19 216	19 193	19 309	19 294	19 329	19 310
	19 254	19 225	—	19 324	—	19 370
+	19 306	19 296	19 403	19 409	19 396	19 403
	19 327	19 320	19 427	19 427	19 414	19 407
$^4G_{9/2}$	—	19 347	19 443	19 443	—	19 440
	13 359	19 354	—	19 460	19 467	19 466
	19 390	19 380	—	19 461	—	19 487
	19 431	19 436	19 551	19 550	—	19 516
	19 554	19 522	19 577	19 581	19 542	19 554
	19 576	19 554	19 616	19 626	19 592	19 575
	—	19 624	19 658	19 667	19 656	19 657
	19 644	19 635	19 690	19 678	19 681	19 676
$^2G1_{9/2}$	—	20 746	—	20 838	—	20 845
	20 779	20 774	20 869	20 850	—	20 851
+	20 838	20 849	—	20 913	20 938	20 916
	20 868	20 888	20 948	20 951	20 952	20 937
$^2D1_{3/2}$	20 905	20 917	20 967	20 960	21 027	20 994
	—	20 973	21 108	21 101	—	21 104
+	21 006	20 997	—	21 112	21 152	21 139
	21 134	21 144	21 241	21 282	21 251	21 277
	21 209	21 230	21 305	21 332	21 325	21 349
$^4G_{11/2}$	21 235	21 250	—	21 360	21 367	21 379
	—	21 252	21 365	21 363	—	21 398
+	21 299	21 323	21 450	21 450	21 410	21 420
	21 393	21 412	—	21 504	—	21 463
$^2K_{15/2}$	21 455	21 477	21 551	21 544	—	21 496
	21 478	21 467	—	21 556	—	21 534
	—	21 502	21 585	21 596	21 561	21 569
	—	21 545	—	21 616	—	21 578
	—	21 551	21 619	21 617	—	21 627
	21 573	21 580	21 651	21 643	—	21 634
	—	21 590	—	21 661	21 677	21 679
	21 604	21 607	21 671	21 683	—	21 682
$^2P_{1/2}$	23 041	23 051	23 155	23 151	23 163	23 156

Table 2. (Continued)

$^{2S+1}L_J$ levels	YVO_4		$YAsO_4$		YPO_4	
	E (exp.)	E (cal.)	E (exp.)	E (cal.)	E (exp.)	E (cal.)
$^2D1_{5/2}$	23 598	23 577	23 682	23 678	23 681	23 696
	23 613	23 627	23 722	23 730	23 710	23 710
	23 638	23 656	23 746	23 749	23 782	23 773
$^2P_{3/2}$	25 939	25 919	26 049	26 045	26 052	26 054
	25 963	25 959	36 088	26 083	26 093	26 083
$^4D_{3/2}$	27 609	27 599	27 856	27 847	27 811	27 794
	27 643	27 642	27 896	27 902	27 914	27 912
$^4D_{5/2}$	—	27 753	27 992	27 979	28 055	28 042
	27 790	27 772	—	28 024	—	28 071
	28 002	27 987	28 230	28 217	28 181	28 172
$^4D_{1/2}$	28 188	28 200	28 448	28 468	28 451	28 478
$^2I_{11/2}$	28 802	28 814	29 007	29 012	—	29 020
	—	28 822	—	29 026	29 042	29 022
	—	28 963	—	29 190	—	29 148
	29 076	29 093	—	29 251	—	29 152
	—	29 124	29 332	29 320	—	29 342
	—	29 196	—	29 344	—	29 358
$^2L_{15/2}$	29 679	29 710	29 884	29 894	29 811	29 782
	29 729	29 724	—	29 904	29 904	29 933
+	—	29 725	—	29 942	—	29 942
	29 769	29 774	29 961	29 984	29 958	29 970
$^4D_{7/2}$	—	29 787	—	30 023	—	30 008
	—	29 790	—	30 042	—	30 039
	—	29 867	—	30 055	30 045	30 047
	29 886	29 884	30 067	30 067	—	30 055
	—	29 913	30 126	30 105	30 152	30 143
	29 944	29 963	—	30 170	—	30 173
	29 990	29 974	—	30 187	—	30 179
	30 070	30 064	—	30 214	30 217	30 197
$^2I_{13/2}$	—	30 259	—	30 443	30 421	30 436
	—	30 264	30 470	30 456	—	30 452
	—	30 347	—	30 553	—	30 523
	—	30 445	30 596	30 601	30 540	30 544
	—	30 474	30 660	30 659	30 596	30 599
	—	30 497	—	30 663	—	30 703
	—	30 541	—	30 696	—	30 717
$^2L_{17/2}$	—	31 235	—	31 422	—	31 628
	—	31 240	—	31 425	—	31 455
	—	31 255	—	31 434	—	31 465
	—	31 257	—	31 449	—	31 472
	—	31 361	—	31 510	—	31 489
	—	31 381	—	31 530	—	31 507
	—	31 386	—	31 548	—	31 522
	—	31 460	—	31 604	—	31 624
	—	31 521	—	31 655	—	31 656
$^2H1_{9/2}$			32 654	32 667	—	32 645
			—	32 707	—	32 664
			—	32 745	—	32 692
			—	32 759	—	32 736
			—	32 815	—	32 800

Table 2. (Continued)

$^{2S+1}L_J$	YVO_4		$YAsO_4$		YPO_4	
levels	E (exp.)	E (cal.)	E (exp.)	E (cal.)	E (exp.)	E (cal.)
$^2D2_{3/2}$			33 086	33 101	33 069	33 092
			33 121	33 121	33 160	33 165
$^2D2_{3/2}$			33 921	33 920	—	33 896
			—	33 980	—	33 974
+			—	33 983	—	34 009
			34 092	34 071	—	34 030
$^2H1_{11/2}$			—	34 117	—	34 040
			—	34 131	—	34 097
			34 162	34 161	—	34 175
			—	34 220	—	34 206
			—	34 263	—	34 263
$^2F2_{5/2}$					38 167	38 168
					—	38 253
					38 250	38 254

parameters) with the three-body interactions. Fourteen free-ion parameters were varied, i.e. E^0, E^1, E^2 and E^3 Racah parameters; α, β and γ Trees parameters, T^2, T^3, T^4, T^6, T^7 and T^8 for the Judd parameters and ζ_{4f}. γ, T^2 and T^8 are fixed to standard values, because these parameters are only important for levels not observed here. Other interactions like spin–spin and spin–other orbit interaction, operating through M^k, P^k parameters, are not included in the simulation, the effect of these interactions being weaker for ions at the beginning of the rare earth series. Following the Wybournes' formalism [13], the crystal field Hamiltonian is expressed as a sum of products of crystal-field parameters and spherical harmonics:

$$H_{CF} = \sum_{k=2}^{4,6} \sum_{q=0}^{k} [B_q^k (C_q^k + (-1)^q C_{-q}^k) + \mathrm{i} S_q^k (C_q^k - (-1)^q C_{-q}^k)]. \tag{2}$$

The number of non-zero crystal-field parameters B_q^k and S_q^k, real and imaginary parts, depends on the site symmetry of the lanthanide ion in the structure. The D_{2d} crystal-field Hamiltonian involves five non-zero real B_q^k crystal-field parameters, namely B_0^2, B_0^4, B_4^4, B_0^6 and B_4^6. The simulation of the energy level scheme was performed on the 96 (102, 90) experimental levels among the 182 possible Kramers doublets of the $4f^3$ configuration, in the case of YVO_4 ($YAsO_4$, YPO_4). With a starting set of phenomenological free ion and cf parameters taken from [14], the rms standard deviation, taken as the figure of merit for the simulation, decreases rapidly to good final values (table 3). However, in their study on Pr^{3+} and Nd^{3+} in YPO_4 and $LuPO_4$ zircon-type hosts, Hayhurst *et al* [15] rejected some lines, supposed to be vibronic side bands. For example, they did not consider the absorption line at 17 351 cm^{-1}, on the high-energy side of the hypersensitive transition $^4I_{9/2} \rightarrow {}^4G_{5/2} + {}^2G_{7/2}$ in Nd:YPO_4. We have observed this line with relatively high intensity at 17 356 cm^{-1} for YPO_4 (figure 4) and this line has been well fitted in our simulation. Similarly the corresponding line (marked with a star in figure 4) was also observed and well fitted by the simulation for Nd:$YAsO_4$ (at 17 344 cm^{-1}) as well as for Nd:YVO_4 (at 17 251 cm^{-1}). This is also in agreement with the $NdVO_4$ absorption spectrum reported in [14]. The simulation performed in [15] took into account only 50 levels whereas we consider here 90 levels. As a

Table 3. Free ion and crystal field parameters for Nd^{3+} ions in YMO_4 (M = V, P, As) single crystals (cm^{-1}). The parameters between square brackets are kept constant during the adjustment and the numbers after the parameters represent the uncertainties. The average crystal field strength (cm^{-1}) is calculated from the energy levels and from the simple overlap model (SOM).

	YVO_4		$YAsO_4$		YPO_4	
Parameters	Phenomological	SOM calculated	Phenomological	SOM calculated	Phenomological	SOM calculated
E^0	23 357 (1)		23 523 (1)		23 520 (1)	
E^1	4757 (1)		4788 (1)		4780 (1)	
E^2	23.05 (0.01)		23.59 (0.01)		23.5 (0.01)	
E^3	478.95 (0.07)		486.94 (0.07)		484.66 (0.07)	
α	20.91 (0.03)		20.69 (0.03)		20.38 (0.03)	
β	−647 (3)		−601 (3)		−602 (3)	
γ	[1500]		[1500]		[1500]	
T^2	[244]		[152]		[202]	
T^3	36 (2)		41 (2)		41 (2)	
T^4	124 (2)		101 (2)		94 (2)	
T^6	−278 (5)		−260 (5)		−262 (5)	
T^7	325 (5)		306 (5)		316 (5)	
T^8	[337]		[138]		[205]	
ξ	869.1 (0.6)		871.4 (0.6)		870.9 (0.6)	
B_0^2	−200 (13)	−312	−164 (13)	−68	240 (9)	436
B_0^4	628 (34)	476	237 (41)	494	108 (38)	503
B_4^4	−1136 (17)	−1405	−1071 (15)	−1371	−1006 (18)	−1303
B_0^6	−1233 (25)	−924	−1043 (27)	−956	−1190 (27)	−903
B_4^6	149 (32)	−237	−10 (27)	178	−90 (27)	3
N_v	2401	2647	2098	2558	2091	2522
Number levels	96		102		90	
σ	16.2		15.4		15.7	

first conclusion, a good agreement between experimental and calculated levels is observed. The mean deviation is 16.2, 15.4 and 15.7 cm^{-1} for YVO_4, $YAsO_4$ and YPO_4 respectively (see table 3).

4.2. Experimental determination of the g factor and comparison with cf calculations

Further tests of the accuracy of the cf parameters can be performed through a comparison of the magnetic properties associated with the lowest $^4I_{9/2}$ Kramers doublet. Indeed, in a crystal field of D_{2d} or lower symmetry, the $^4I_{9/2}$ energy level splits into five Kramers doublets. The first excited Stark level being 110 cm^{-1} above the fundamental one, only the ground level is populated at liquid helium temperature. Under an external magnetic field, this doublet splits into two levels and, according to the usual interpretation of the electron paramagnetic resonance (EPR) theory, this system can be described as having an effective spin of $S = 1/2$. Using a fitting procedure for all the different transitions observed at different angles [18], the spin Hamiltonian parameters are determined and reported in table 4. The results are similar to those previously reported [16, 17]. From the experimental g-tensor principal values, the wave functions of the lowest Kramers doublet can be obtained assuming that the term-mixing and the J-mixing are negligible (the lowest Kramers doublet

Table 4. Experimental and calculated spin Hamiltonian parameters and wave function composition extracted from the crystal field calculations and from EPR measurements in Nd:YMO_4 (M = V, P, As).

	g-factor values			Calculated wave function composition	
YMO_4	Calculated from CFC	Experimental from EPR	Difference (%)	From cf [a]	From EPR
YVO_4	$g_\parallel = 0.94$	$g_\parallel = 0.915 \pm 0.004$	3	$64\%\|{}^4I_{9/2}, \frac{1}{2}\rangle$	$71\%\|{}^4I_{9/2}, \frac{1}{2}\rangle$
	$g_\perp = 2.46$	$g_\perp = 2.361 \pm 0.003$	4	$31\%\|{}^4I_{9/2}, -\frac{7}{2}\rangle$	$28\%\|{}^4I_{9/2}, -\frac{7}{2}\rangle$
				$1.7\%\|{}^2H_{9/2}, \frac{1}{2}\rangle$	$1\%\|{}^4I_{9/2}, \frac{9}{2}\rangle$
$YAsO_4$	$g_\parallel = 1.63$	$g_\parallel = 1.874 \pm 0.002$	13	$50\%\|{}^4I_{9/2}, \frac{1}{2}\rangle$	$54\%\|{}^4I_{9/2}, \frac{1}{2}\rangle$
	$g_\perp = 2.16$	$g_\perp = 1.938 \pm 0.001$	12	$45\%\|{}^4I_{9/2}, -\frac{7}{2}\rangle$	$45\%\|{}^4I_{9/2}, -\frac{7}{2}\rangle$
				$2\%\|{}^4I_{9/2}, \frac{9}{2}\rangle$	$1\%\|{}^4I_{9/2}, \frac{9}{2}\rangle$
YPO_4	$g_\parallel = 2.90$	$g_\parallel = 3.101 \pm 0.005$	6	$65\%\|{}^4I_{9/2}, -\frac{7}{2}\rangle$	$66\%\|{}^4I_{9/2}, -\frac{7}{2}\rangle$
	$g_\perp = 1.42$	$g_\perp = 1.217 \pm 0.007$	17	$28\%\|{}^4I_{9/2}, \frac{1}{2}\rangle$	$33\%\|{}^4I_{9/2}, \frac{1}{2}\rangle$
				$2\%\|{}^4I_{9/2}, \frac{9}{2}\rangle$	$1\%\|{}^4I_{9/2}, \frac{9}{2}\rangle$

[a] Only the three principal components are taken into account.

is supposed to be purely $^4I_{9/2}$). This could be experimentally verified, if the $A_\parallel g_\perp / A_\perp g_\parallel$ ratio is very close to one [19]. In our measurements, these ratios are 1.1 for YVO_4, 1.0 for $YAsO_4$ and 1.0 for YPO_4 [18]. The wave functions of the lowest Kramer doublet are reported in table 4.

Alternatively, these $g_\parallel$ and $g_\perp$ EPR parameters and the wave functions of the lowest Kramers doublet of the $^4I_{9/2}$ manifold can be calculated using the cf parameters. This can be done by including the magnetic interaction through the $L + g_e S$ tensor operator, either included in the Hamiltonian before the secular determinant diagonalization, or as a perturbation operating on the ground state wave function. The latest approximation is used in this calculation and the results are gathered in table 4. A rather small discrepancy (average value of 9%) is obtained between the experimental and the theoretical g-tensor principal values. The results are even better with the wave function composition, as a 7% discrepancy is obtained for Nd:YVO_4, 4% and 5% for Nd:$YAsO_4$ and Nd:YPO_4 respectively. The cf calculation requires no assumption concerning the mixing. It is therefore possible from these calculations to verify the absence of J-mixing and term-mixing. As reported in table 4, only in the case of Nd:YVO_4 a 2% value of term mixing ($^2H_{9/2}$ level) is observed while, for the two other hosts, the wave function has a purely $^4I_{9/2}$ character.

4.3. Calculation of the crystal field parameters by the simple overlap model

The simple overlap model (SOM) developed by Malta [20] has been previously applied to reproduce the phenomenological cf parameters of a great number of lanthanide and 3d compounds [21]. The SOM supposes that the crystal field effect can be calculated using a potential produced by an effective charge distribution over a small region, situated around the mid-point of the metal–ligand distance. It calculates the B_q^k parameters with the relation:

$$B_q^k = \rho \left(\frac{2}{1 \pm \rho} \right)^{k+1} A_q^k \langle r^k \rangle \tag{3}$$

where A_q^k is the lattice sum of neighbours belonging to the first coordination sphere associated with an effective charge, $\langle r^k \rangle$ are the radial integrals [22], ρ is the overlap

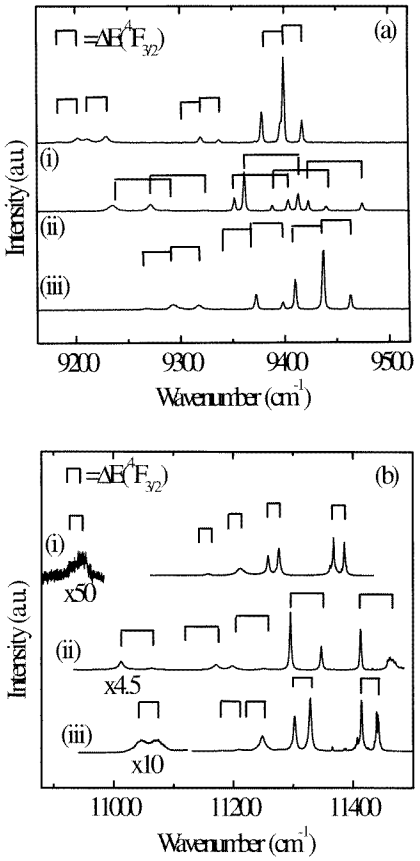

Figure 3. Fluorescence spectra of Nd^{3+} ions at 10 K in (i) YVO_4, (ii) YPO_4, (iii) $YAsO_4$. (a) $^4F_{3/2} \rightarrow {}^4I_{9/2}$ transition, (b) $^4F_{3/2} \rightarrow {}^4I_{11/2}$ transition.

between the 4f orbital of the central ion and the s and p orbitals of the ligand, the value of which varies as a function of the metal–ligand distance R: $\rho = \rho_0(R_0/R)^{3.5}$, R_0 being the shortest metal–ligand distance. For the rare earth, ρ lies between 0.04 and 0.08 [21]. The $\pm$ sign in equation (3) characterizes the displacement of the charge barycentre from the middle of the metal–oxygen distance [22]. When applied to the isostructural series here studied, a good agreement is obtained for the cf values (see table 3) as well as for their variation as a function of the unit cell parameters of YMO_4 (M = V, As, P). An effective charge of -0.8 for the oxygen and an overlap of 0.04 is found, which indicates a relatively covalent Nd–O bonding.

This demonstrates that an *a priori* calculation can be performed with the knowledge of the coordination, the site symmetry and the distances between the RE^{3+} and the first coordinated neighbours. It is then possible to estimate the magnitude of the crystal field strength.

4.4. Crystal field strength

It has been shown previously that there is a good agreement between experimental and calculated energy level diagrams for the three neodymium activated hosts. The similarities

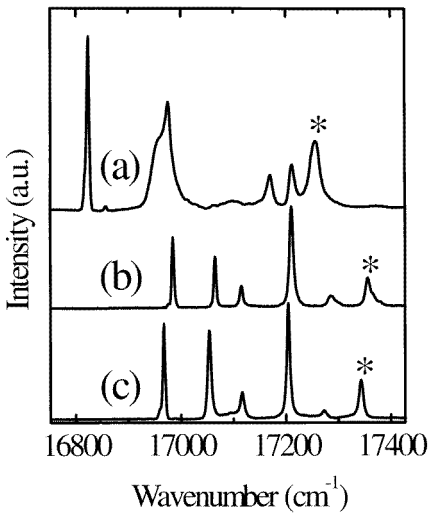

Figure 4. Nd^{3+} ions $^4I_{9/2} \rightarrow {}^2G_{7/2} + {}^4G_{5/2}$ absorption spectra at 10 K in (a) YVO_4, (b) YPO_4, (c) $YAsO_4$. The lines labelled by a star are taken into account in our simulation but not in [15].

of the g-factors and ground state Kramers wave functions, deduced from the cf calculation and measured by EPR, confirm that the sets of crystal field parameters given in table 3 describe accurately the behaviour of Nd^{3+} in YMO_4 matrices. This allows going further into a discussion of the structure–crystal field strength relationship.

For the three hosts, the crystal field strength can be estimated according to [23]:

$$N_v = \left[\sum_{k \neq 0, q} \frac{4\pi}{2k+1} (B_q^k)^2 \right]^{1/2}. \tag{4}$$

The values reported in table 3 are calculated from the two sets of crystal field parameters respectively deduced from the energy level diagram and calculated with the SOM theory. A very good agreement between experimental and calculated N_v parameters (less than 18% discrepancy) is obtained; N_v slightly increases from YPO_4 to $YAsO_4$. A comparison of the structural parameters (table 1) and the N_v values indicates that there is no simple relation between the mean O–Y distances and the N_v parameters. It means that the bond angles may have a predominant effect.

Another very important characteristic of these specific crystal-field materials is that they correspond to low self-quenching compounds [23]. In general, high activator Nd^{3+} concentration leads to poor quantum efficiency for emission as Nd^{3+}–Nd^{3+} interactions, generally by non-radiative energy transfer (energy migration, cross relaxation), are in competition with the radiative emission. These energy transfers are reduced when the overlap corresponding to the transitions $^4F_{3/2} \rightarrow {}^4I_{15/2}$ and $^4I_{9/2} \rightarrow {}^4I_{15/2}$ is small [23, 24]. It is the case in the low crystal field strength compounds.

5. Conclusion

In this study, the crystal field analysis of Nd^{3+} ions substituted in three zircon type hosts is reported. Crystals have been synthesized under the same experimental conditions, using a flux method. A good agreement is obtained between the cf parameters adjusted from the

experimental optical absorption measurements and those calculated using the simple overlap model.

Electron paramagnetic resonance is also used to probe the accuracy of the crystal field calculations. The correlated energy level diagrams for each host allow to identify the extra lines of the absorption spectra that are not accounted for by purely electronic transition and are, mainly, of vibronic origin.

A low crystal field strength appears to be a clue for laser materials as a very important consequence is the resulting high values of the absorption cross sections. Several Stark sub-levels of the Nd^{3+} $^4I_{9/2}$ ground state are gathered in a very narrow energy range and at room temperature, when several of these sublevels are populated, a large number of transitions overlap, leading to a very high absorption coefficient. For sake of comparison, the cf strength is twice higher in the Nd:YAG than in the Nd:YVO_4 and this leads to an absorption cross section six times larger in the latter compound. This leads to a lower overlap of the energy levels engaged in the luminescence processes, and therefore to a lower quenching of the Nd^{3+} luminescence.

Finally, Nd:YPO_4 and Nd:$YAsO_4$ materials present spectroscopic properties very close to Nd:YVO_4 ones. Therefore further investigation of these two hosts which may also exhibit interesting laser properties should be performed in the future.

References

[1] Feugnet G, Bussac C, Larat C, Schwarz M and Pocholle J P 1994 *Opt. Lett.* **20** 157
[2] Bernard J E and Alcock A J 1993 *Opt. Lett.* **18** 968
[3] Matthews D G, Boon J R, Conroy R S and Sinclair B D 1996 *J. Mod. Opt.* **43** 1079
[4] Chai B H T, Loutts G, Lefaucheur J, Zhang X X, Hong P, Bass M, Shcherbakov I A and Zagumennyi I A 1994 *OSA Proc. Adv. Solid State Laser* **20** 41
[5] Anderson F G, Summers P L, Weidner H, Hong P and Peale R E 1994 *Phys. Rev.* B **50** 14 802
[6] Guillot-Noël O, Viana B, Aka G, Kahn-Harari A, Gourier D and Vivien D 1997 *J. Lumin.* **72** 195
[7] Wanklyn B M 1981 *J. Cryst. Growth* **54** 610
[8] Smith S H and Wanklyn B M 1974 *J. Cryst. Growth* **21** 23
[9] Antic-Fidancev E, Lemaître-Blaise M and Caro P 1984 *C. R. Acad. Sci., Paris* **298** 575
[10] Antic-Fidancev E, Lemaître-Blaise M, Caro P, Piriou B and Strek W 1985 *Proc. Int. Symp. on Rare Earth Spectroscopy* (Wroclaw: World Science) p 354
[11] Guillot-Noël O 1997 *These de l'Université P et M Curie Paris 6*
[12] Carnall W T, Goodman G L, Rajnak K and Rana R S 1989 *J. Chem. Phys.* **90** 3443
[13] Wybourne B G 1965 *Spectroscopic Properties of Rare Earths* (New York: Wiley)
[14] Antic-Fidancev E, Hölsä J, Lemaître-Blaise M and Porcher P 1991 *J. Phys.: Condens. Matter* **3** 6829
[15] Hayhurst T, Shalimoff G, Conway J G, Edelstein N, Boatner L A and Abraham M M 1982 *J. Chem. Phys.* **76** 3960
[16] Ranon U 1968 *Phys. Lett.* **28A** 228
[17] Abraham M M, Boatner L A, Ramey J O and Rappaz M 1983 *J. Chem. Phys.* **78** 3
[18] Guillot-Noël O, Simons D and Gourier D 1998 *J. Phys. Chem. Solids* submitted
[19] Abragam A and Bleaney B 1971 *Résonance Paramagnétique Électronique des Ions de Transition* vol 5 (Paris: Presses Universitaires de France) p 317
[20] Malta O L 1982 *Chem. Phys. Lett.* **87** 27
Malta O L 1982 *Chem. Phys. Lett.* **88** 353
[21] Porcher P, Couto dos Santos M and Malta O L 1998 unpublished results
[22] Freeman A J and Desclaux J P 1979 *J. Magn. Magn. Mater.* **12** 11
[23] Auzel F 1980 *Radiationless Processes* ed B Di Bartolo **B-62** p 213
[24] Viana B, Lejus A M, Saber D, Duxin N and Vivien D 1994 *Opt. Mater.* **3** 307